Intercomparison of Model Simulations of the Impact of 1997/98 El Niño on South American Summer Monsoon

Jiayu Zhou

Goddard Earth Sciences and Technology Center, University of Maryland
Baltimore, MD 21250

and

K.-M. Lau

Climate and Radiation Branch, Laboratory for Atmospheres
NASA/Goddard Space Flight Center
Greenbelt, MD 20771

Submitted to *Meteorologica* Special Issue
on Variability of the South American Monsoon System

March 2002

Corresponding author address: Dr. Jiayu Zhou, GEST, Code 913, NASA/GSFC, Greenbelt, MD 20771
E-mail: zhou@climate.gsfc.nasa.gov

Intercomparison of Model Simulations of the Impact of 1997/98 El Nino on South American Summer Monsoon

Jiayu Zhou[1], and K.-M. Lau[2]

Submitted to Meteorologica Special Issue on Variability of the South American Summer Monsoon

Popular Summary

Our previous observational study on the impact of 1997/98 El Niño on the South American summer monsoon (SASM) showed a major reduction of rainfall over the Amazon associated with a poleward shift of the SASM circulation and rainfall system during 1997/98 austral summer. A much stronger low-level northwesterly jet was found along the eastern side of the subtropical Andes and an enhanced upper tropospheric high over the Altiplano Plateau. Both were in response to the positive tropospheric temperature anomaly expanding from the central Pacific to tropical-subtropical South America.

In this study, we have evaluated the atmospheric general circulation model (AGCM) simulations of climatology and response of the SASM to the 1997/98 El Niño, using an ensemble of two-year (September 1996 - August 1998) integration provided by the CLIVAR Asian-Australian Monsoon Atmospheric Model Intercomparison Project. The study is important to the understanding of aforementioned large-scale El Niño impacts and to the improvement of the regional climate prediction via dynamical downscaling from large-scale climate models.

The model simulations of the climatology show that the stationary pressure systems and the seasonal cycle are overestimated. Large systematic rainfall errors are found in association with the Andes and the Atlantic intertropical convergence zone, indicating model problems in handling steep mountains and parameterization of convective processes. The seasonal development of the monsoon rainfall system shows large variability among AGCMs.

Regarding the impact of 1997/98 El Niño anomaly, most models can simulate the large-scale tropospheric warming response over the tropical central-eastern Pacific, but the response becomes too weak over subtropical South America. As a result, the Bolivian high is less enhanced in the simulation. Most models fail to simulate the strengthening of the northwesterly low-level jet (LLJ) along the eastern foothills of the Andes. Due to lack of moisture transport from Amazon basin by the northwesterly LLJ, the positive rainfall anomaly center observed over the Uruguay-Southern Brazil area is missing in all six AGCM simulations.

The assessment of the predictability of regional rainfall anomaly shows promising skill over northern Brazil and Ecuador coast, where is directly under the influence of the Walker cell shift in response to the SST warming in the eastern-central Pacific, but not over the subtropical southeast of South America, where the anomaly is generated by the El Niño induced regional feedback processes and complex interactions with subcomponents of SASM and mid-latitude systems, which are dependent on the internal dynamics of the SASM.

[1]UMBC/Goddard Earth Sciences and Technology Center

[2]NASA/Goddard Space Flight Center

ABSTRACT

The simulations of climatology and response of the South American summer monsoon (SASM) to the 1997/98 El Niño are investigated using six atmospheric general circulation models. Results show all models simulate the large-scale features of the SASM reasonably well. However, both stationary and seasonal components of the surface pressure are overestimated, resulting in an excessively strong SASM in the model climatology. The low-level northwesterly jet over eastern foothills of the Andes is not well resolved because of the coarse resolution of the models. Large rainfall simulation biases are found in association with the Andes and the Atlantic ITCZ, indicating model problems in handling steep mountains and parameterization of convective processes.

The simulation of the 1997/98 El Niño impact on SASM is examined based on an ensemble of ten two-year (September 1996 - August 1998) integration. Results show that most models can simulate the large-scale tropospheric warming response over the tropical central Pacific, including the dynamic response of Rossby wave propagation of the Pacific-South America (PSA) pattern that influences remote areas. Deficiencies are found in simulating the regional impacts over South America. Model simulation fails to capture the southeastward expansion of anomalously warm tropospheric air. As a result, the upper tropospheric anomalous high over the subtropical Andes is less pronounced, and the enhancement of subtropical westerly jet is displaced 5°-10° equatorward compared to the observed. Over the Amazon basin, the shift of Walker cell induced by El Niño is not well represented, showing anomalous easterlies in both upper and lower troposphere. In association with the simulation of weaker sinking motion over Northeast Brazil, the low-level anti-cyclonic couplet over the Amazon basin is obscured. The observed strong LLJ anomaly along the eastern foothills of the subtropical Andes is not

simulated by all models. Consequently, the rainfall anomaly over Uruguay and Southern Brazil is missing in all model simulations.

Based on the inter- and intra-ensemble variability our study reveals that the regional rainfall anomaly over northern Brazil and Ecuador coast is more predictable than that over Uruguay and Southern Brazil. The former is influenced by the Walker cell shift as a direct response to El Niño, and the latter by the indirect response to El Niño, involving regional feedback processes and internal variability among SASM subcomponents and mid-latitude systems.

1. Introduction

The South American summer monsoon (SASM) has been recognized as a major climate system over South America in austral summer (reviewed by Nogués-Paegle *et al.* 2002), whose interannual variability is strongly influenced by the El Niño-Southern Oscillation (ENSO). Previous studies showed that a typical response of the SASM to El Niño has the following large scale features: an equatorward displacement of low-level monsoon perturbation easterlies as a result of the Walker cell shift; the enhancement of northwesterlies along the eastern foothills of the Andes; predominant drought condition over north-northeastern Brazil, and flood conditions over southeastern subtropical South America and the Ecuador coast (Kousky *et al.* 1984; Aceituno 1988; Ropelewski and Halpert 1987; Douglass *et al.* 1999; Grimm *et al.* 2000; Zhou and Lau 2001). In individual El Niño year, the response may vary due to the influences of subseasonal variations and decadal to multi-decadal variability. (Garreaud and Wallace 1998; Uvo *et al.* 1998; Liebmann *et al.* 1999; Zhou and Lau 1999; Nogués-Paegle *et al.* 2000).

In a recent study, Lau and Zhou (2002, hereafter referred to as LZ) observed a major reduction of rainfall over the Amazon associated with a poleward shift of the SASM circulation and rainfall system during the 1997/98 El Niño. They showed that the Bolivian high was hydrostatically enhanced by the anomalous tropospheric warm ridge extending from the Niño-3 region to the Altiplano Plateau. They found a much stronger low-level jet (LLJ) penetrated deeply into the extratropics along the eastern side of the subtropical Andes, coinciding with the reinforcement of the upper tropospheric subtropical westerlies and the local meridional overturning. They further demonstrated that an important difference between the 1997/98 anomaly and the typical El Niño impact was that the South Atlantic subtropical high anomaly was split into two low-level centers, one immediately to the south of the Amazon Basin and the

other over the southeastern Atlantic. It is found that the SASM anomalies during 1997/98 may also be affected by teleconnection signals linking the South Pacific and the South Atlantic in December, January and February (DJF) of 1997/98.

The results of LZ have motivated the authors to evaluate how well state-of-the-art atmospheric general circulation models (AGCM) can simulate the response of SASM to ENSO. This issue is not only important to the understanding of the aforementioned large-scale ENSO impacts but also to the improvement of the regional climate prediction via dynamical downscaling from large scale climate models. A number of recent studies showed that the effectiveness of seasonal regional climate prediction, based on high-resolution regional model embedded in a coarse-resolution AGCM, is highly dependent on the large-scale environment predicted by the AGCM (Nobre *et al.* 2001). In this paper we present results of a model intercomparison study, which uses six AGCMs to assess the model simulation of the 1997/98 El Niño impact on SASM. A description of participating AGCMs and the experimental design are given in Section 2. The model simulations of the SASM climatology are intercompared in Section 3. The responses of the model SASM to the 1997/98 El Niño, including an assessment of predictability of regional precipitation are discussed in Section 4. Finally, a summary is presented in Section 5.

2. Data and experimental design

The atmospheric general circulation model output used in this study were provided by the CLIVAR Asian-Australian Monsoon AGCM Intercomparison Project (Kang *et al.* 2002). Six AGCMs with comparable resolutions were chosen, *i.e.* the Center for Ocean-Land-Atosphere Studies model (COLA), the NASA/ Goddard Earth Observing System model (GEOS), the Geophysical Fluid Dynamics Laboratory model (GFDL), the National Center for Atmospheric

Research model (NCAR), the NCEP model and the State University of New York / Goddard Laboratory for Atmospheres model (SUNY/GLA). Among them, four are spectral models and the other two are grid models. The physics packages used by each model are listed in Table 1. Except for the GEOS model, each model provided a climatology of monthly means from an extended integration of Atmospheric Model Intercomparison Project (AMIP) (Gates *et al.* 1999) from 1 January 1979 to 31 December 1998. The GEOS model climatology is for a shorter period of 1980-1992. To assess predictability an ensemble of ten two-year runs for the period from 1 September 1996 to 31 August 1998 were carried out for each model. This period covers the 1997/98 El Niño episode from initiation to termination. Ten model integration were carried out for each model with initial conditions of 1 September chosen from different years of the extended long-term AMIP integration. For boundary conditions, the sea surface temperature (SST) data are the observed pentad mean from the global sea-ice and SST data from the UK Meteorological Office (Folland and Parker, 1995) and others are the same as that used in AMIP. The Climate Prediction Center Merged Analysis of Precipitation (CAMP) data (Xie and Arkin, 1997) and the National Center for Environmental Prediction (NCEP) reanalysis (Kalnay *et al.* 1996) with the recent correction of the satellite temperature data over land were used for validation. The horizontal resolution for both data sets is 2.5° latitude × 2.5° longitude. Because only 200 and 850 hPa data of GEOS simulation were available to us, the following discussion on vertical structures of wind and temperature does not include the result of GEOS simulation.

3. Simulation of SASM climatology

The impact of systematic error on the model response to anomalous lower boundary forcing has been addressed by a number of studies (*e.g.*, Shukla and Fennessy 1994). In this section, the SASM climatologies, as simulated by the AGCMs, are evaluated.

a. Pressure and circulation systems

Figures. 1(a) and (b) show the NCEP reanalysis and the ensemble model-minus-observation differences of the annual mean sea level pressure (SLP) and low-level wind systems, respectively. We can see that the stationary systems of both North and South Atlantic subtropical highs and the Amazonia low are too strong compared to observation, indicating large influences of geographical distribution of the ocean and continent on the model annual mean biases. The same figures but for the DJF seasonal mean departure are displayed in Fig. 1(c) and (d). The observation shows that from austral winter to summer, sea level pressure (SLP) increased over northwest Africa and decreased over Gran Chaco of South America, exerting an anomalous pressure gradient force from the northeast to the southwest in the tropical and subtropical area between 80°W and 20°E. As a result, the seasonal monsoon flow (departure from annual mean) shows enhanced north equatorial trade winds and the north-northwesterlies east of the Andes north of 15°S. Again, model simulations over-estimate the northwestern African high and the Gran Chaco low, which also moves toward the central Andes (Fig.1 (d)), exaggerating the austral summertime pressure gradient and producing too strong low-level perturbation monsoonal wind along the equatorial North Atlantic and over the east of the Andes. Because the Andes in the model is much lower and smoother than that in the real world, the excessive low pressure over the central Andes in the simulation also draws enormous westerlies from the equatorial eastern Pacific, which cross the Andes and turn southward toward the low. The easterlies over the equatorial eastern Pacific are totally reversed and the LLJ east of the Andes strengthened anomalously.

One of the critical features linking the SASM to the climate of subtropical South America (southern Brazil and the Rio de la Plata basin) is the low level jet (LLJ), which transports moisture from lower latitudes to subtropical South America (Virji 1981; Paegle 1998; Berbery

and Collini 2000). The NCEP reanalysis climatology shows there are two branches of low-level northerlies, one along the eastern foothills of the Andes and the other near the southeast coast of Brazil (Fig. 2(a)). The former is strong, displaying north-northwesterlies throughout the year. While the latter, situated between the Gran Chaco low and the South Atlantic high, is weaker than the western counterpart and has distinct annual cycle. Both jets have northerly maxima around 15°S in austral summer. It is also noticed that the western jet core shifts equatorward about 5-10° latitudes from austral winter to summer in response to the reversal of the seasonal perturbation wind around the Gran Chaco low (not shown). The ensemble simulation (Fig. 2(b)) captures the enhancement of northerlies close to the eastern Andes and over the east coast during austral summer. Due to the coarse resolution of the models, large errors of wind speed are found between the two jet cores around 50°-60°W. The western jet is too weak during the austral winter half year. Large standard deviations among model simulations (darkly shaded) are found in alignment with two jet maxima, indicating the variations of two jets are also model dependent in the model climatology.

Over the east coast of Brazil, the NCEP reanalysis (Fig. 3(a)) reveals a distinct local Hadley cell in the summer season with the strong upper-tropospheric return flow (southerlies), which is associated with the anticyclonic circulation over the Altiplano Plateau, overlying the low-level northerlies. Because the data at 150-hPa are unavailable for most model outputs (except for the NCEP model), the simulated upper-level return flow center shifts from 150 to 200-hPa (Fig. 3(b)). Otherwise, the temporal evolution of the meridional overturning is fairly well simulated, showing development between September and October, peak in December and demise around April. Over the eastern subtropical Andes (around 15°S), the observation (Fig. 3(c)) shows that low-level northerlies prevail throughout the year, and are confined below 700-hPa in DJF but extend to higher level in the austral winter half year. Compared with the

observation, the simulation (Fig. 3(d)) shows too strong upper-tropospheric southerlies in austral summer and significant weakening of northerlies in austral winter, when anomalous southerlies are resulted in the model upper-troposphere.

b. Rainfall distribution and evolution

Compared to the CMAP rainfall analysis, both annual and seasonal mean rainfall simulations have similar systematic bias towards excessive rainfall over the tropical-subtropical Andes and deficient precipitation in the Atlantic Inter-tropical Convergence Zone (ITCZ) (Fig. 4 shows the seasonal means). Further examination of the standard deviation among model simulations reveals that the areas with large errors also have large variations (not shown), indicating that the error amplitude of simulations could be model dependent. Figure 5 shows individual model results for DJF. By and large, four spectral models have larger errors over the tropical-subtropical Andes but smaller over the Atlantic ITCZ, while two grid models do quite the contrary. We speculate that the model problems could arise from the representation of steep mountains and the parameterization of convective processes. More diagnostic studies and model tests are needed to fully understand the causes of these problems. Despite the above systematic errors in SASM rainfall simulation, the proportion of the seasonal rainfall amount, measured by the percentage of the annual sum for each season, is found to be reasonably well simulated by the ensemble mean compared to the CMAP rainfall analysis (Fig. 6). In DJF, the geographic extent of 40% contour captures the summer monsoon rainfall regime.

The development of South American summer rainfall shows two distinct regimes, *i.e.* the continental SASM regime and the western Atlantic ITCZ regime (Zhou and Lau 2001). Each regime has distict seasonal characteristics. The CMAP rainfall (Figs. 7 (a) and (b)) shows that over the tropical-subtropical South American continent, heavy rainfall (as represented by the 6 mm/day contour) progresses from the northwest toward the southeast from September to

January. In November, the heavy rain zone jumps poleward by almost ten-degree latitude signaling the SASM onset. The monsoon rain belt continuously moves southward and expands toward the east and the west until January. Subsequently, the heavy rainfall area shrinks and retreats back toward the equator. Figures 7 (c) and (d) show the result of model ensemble mean variation, which captures reasonably well the rainfall advancement and withdrawal over the central-eastern continent, but shows spurious heavy rainfall over the subtropical Andes from September to following April. Over the tropical western Atlantic, the ITCZ continuously moves southward from spring to fall. In April, it reaches to the southernmost position and connects with the continental rainfall system, forming a continuous precipitation band from western Atlantic to central Amazon. Those aforementioned features are captured by the model ensemble simulation except that the model heavy rain is more confined to the area close to the continent after January (Fig. 7d). In general, the results indicate that models, having better mean rainfall simulation over land, e.g., GEOS AGCM, show more realistic migration over the South American continent; while models with better tropical oceanic mean rainfall, e.g., GFDL AGCM, do better over the tropical western Atlantic (not shown). These results are consistent with their individual model bias.

In summary, the models overestimate the strength of the stationary systems and the seasonal variation relative to the observation. Large rainfall systematic errors are related to the presences of the Andes and convective activities over the Atlantic ITCZ. The simulation of LLJs east of the Andes is problematic, because of coarse model resolution. Despite all these defects, some SASM characteristics, *i.e.* the seasonal rainfall fraction, the seasonal migration of monsoon rainfall over the eastern continent, the enhancement of low level northerlies east of the Andes in the summer season and the evolution of local Hadley circulation over the east coast, are

simulated reasonably well. All these model problems and capabilities could affect the simulation of the ENSO-SASM relationship.

4. Simulation of 1997/98 El Niño impact on SASM

In the following, we focus on the model simulation of the 1997/98 El Niño impact on SASM.

1. Thermal impact

In this section, we examine the changes in tropospheric temperature associated with the SASM during DJF 1997/98. Figure 8 shows the vertical cross-section of temperature anomaly along 15°S. Observation reveals that in DJF 1997/98 warming in the Niño 3 region extended from the surface and intensified upward with maximum warming in the upper troposphere near 300-400 hPa. The mid-upper troposphere warming expanded eastward and also downward, forming a secondary warming center at 600 hPa around 100°W. As a result, the temperature above the Altiplano Plateau increased significantly. Overall, this feature is captured by the ensemble simulation, except for the absence of the secondary center. However, large differences, indicated by the shading of standard deviations, can be seen among model simulations. Figure 9 shows the individual model simulations, which reveal that the COLA and NCAR GCMs have the mid-tropospheric anomalies displaced too far eastward, while the temperature anomaly in the NCEP GCM does not extend eastward enough. The GFDL and GLA models have about the right thermal structure as the observed over South America.

Figure 10 shows the impact of anomalous warming on the geographic distribution of 200-hPa geopotential height. Constrained by the hydrostatic relationship between temperature and geopotential height, NCEP reanalysis reveals two positive anomalous height centers in the tropical eastern Pacific straddling the equator and extending northeast-and-southeastward. The

southern branch reaches the Altiplano Plateau and intensifies the Bolivian High, consistent with the vertical structure of temperature anomaly discussed above. The model ensemble mean correctly captures the position and the strength of the two anomaly centers over the tropical eastern Pacific, as evident in the small error relative to the observation (Fig. 10b). Large negative errors (<-10m) seen over the Gulf of Mexico and the subtropical Andes (20°-30°S) indicate that models are deficient in simulating the northeast and southeastward extention of the upper tropospheric height anomalies, which is consistent with the insufficient middle-upper tropospheric warming simulated by the model over the two regions. Small standard deviations shown over the subtropical South America (light shadings) indicate this problem is common to all model simulations.

b. Dynamical response

The dynamical response to the positive SST anomaly over the eastern equatorial Pacific during 1997/98 El Niño is examined in Fig. 11, which shows respectively the 200- and 850-hPa streamline and wind anomalies. NCEP reanalysis (Fig. 11(a) and (b)) shows distinct upper tropospheric Rosbby wave trains, excited by the warming over the equatorial eastern Pacific, creating the well-known Pacific-North America (PNA) and Pacific-South America (PSA) patterns over the western hemisphere (Wallace and Gutzler 1981; Mo and Nogués-Paegle 2001). The vertical structure of the perturbation is highly equivalent barotropic in high latitudes and baroclinic in low latitudes. Overall, the model ensemble simulations (Fig. 11(c) and (d)) capture those features quite well, but the wave pattern is smoother and the strength of wind anomaly much weaker than that shown in NCEP reanalysis on both upper and lower levels (also see Kang *et al.* 2002). Far from the source, the wave train centers are shifted, especially over the Southern Hemisphere. The anomalous anticyclonic circulation, which enhances the South Atlantic

subtropical high southwest of South Africa, is displaced northeastward to the South African continent (Fig. 11 (d)).

For the regional response, the observation shows a pair of distinct lower tropospheric anticyclones (shown in the square of Fig. 11(b)) forced by the intense subsidence over northeastern Brazil straddles the equator over tropical South America. The shift of Walker circulation is represented by strong anomalous lower-level westerlies and upper-level easterlies over the eastern equatorial Pacific and anomalous winds in reverse directions over the Amazon Basin. As a result, abnormal low-level convergence and upper-level divergence are found over the Ecuador coast (Figs. 11(a) and (b)). In the model ensemble simulation, deficiencies can be clearly seen over tropical South America, where the low-level anti-cyclonic and upper-level cyclonic couplets are barely visible, implying much weaker anomalous sinking motion over northeastern Brazil in the simulation. The Walker cell anomaly over Amazon is erroneously replaced by weak easterly anomalies throughout the troposphere (Figs. 11(c) and (d)). In the low-level, anomalous equatorial easterlies cross over the Andes, breaking away from the flow turning southeastward. It significantly weakens the anomalous northwesterlies along the eastern foothills of the Andes.

In the vertical extent. NCEP reanalysis (Fig. 12(a)) shows substantial enhancement in the vertical westerly shear, induced by significant increase of the temperature gradient between the tropics and the extratropics. The westerly anomaly maximum is located at 30°S around 150-hPa and the ridge extends downward through the troposphere. A secondary westerly anomaly center, which is separated from the upper tropospheric maximum, is found at 17°S around 700-hPa (Fig.12(a)). This center occurs in conjunction with the enhancement of the northwesterly LLJ east of the Andes (see also Fig. 13(a)). Comparing with the reanalysis, the simulated upper

tropospheric maximum center (Fig. 12(b)) is about 2 m/s weaker and shifted almost 5° equatorward, consistent with the simulation error of the upper tropospheric cyclonic turning over the central Andes (Fig. 11(c)) induced by the inadequate warming expanded from the tropical central-eastern Pacific. The simulation does not capture the weak westerly anomaly center at 700-hPa, only showing a vertical ridge declining equatorward. Small standard deviations along the observed maximum axis and over the 700-hPa center indicate similar deficiencies also exist in individual model simulation. Substantial differences among model simulations are found along the simulated ridge, on which large standard deviations are superimposed.

Figure 13 shows the vertical extent of meridional wind along 15°S. In the observation (Fig.13 (a)), strong anomalous northerlies of more than 4 m/s are centered between 850 and 700-hPa and vertically extended upward beyond 400-hPa over the eastern foothills of the tropical-subtropical Andes. The models poorly simulate the strength of the anomalous LLJ with only about one tenth of the observed intensity (Fig.13 (b)). Small standard deviations among models are found aligning with the maximum axis, suggesting all models have similar problem. Substantial variability among model simulations indicated by large standard deviation can be seen around 63°-58°W at 850 hPa.

c. Rainfall anomaly and predictability

The model ensemble simulations of precipitation and 850-hPa wind anomalies are presented in Fig.14, showing that the enhancement of rainfall off the Ecuador coast is reasonably well-simulated. The models also tend to produce reduced precipitation over the Atlantic ITCZ and northern South America with less severity. In Fig.14 (a), the observation demonstrates that the equatorial low-level easterly anomalies, channeled by the steep Andes Mountain, turn sharply southeastward and significantly enhance the northwesterlies along foothills of the eastern Andes.

The model ensemble simulation fails to simulate this feature; hence there is no increased moisture transport, leading to complete missing of positive rainfall anomaly center over Uruguay-Southern Brazil region (Fig.14 (b)).

Intercomparing among model results (Fig.15), we can see the simulations of rainfall anomalies over the Atlantic ITCZ and the Ecuador coast are quite consistent, but the flow anomalies and the associated rainfall over subtropical South America are incongruous. The NCEP model simulates neither strong anomalous easterlies over the Amazon basin nor northeasterly anomalies along the eastern foothills of the subtropical Andes (where weak southerlies are found). The GLA model creates strong equatorial east-southeasterly anomalies, which cross over the tropical Andes and dominate over the equatorial eastern Pacific. The COLA and GFDL model simulations show strong anomalous northeasterlies over Amazon, which impinge the Andean mountain between the equator and 15°S and result in expansion of excessive rainfall from the Ecuador coast to the subtropical Andes south of 10°S. From GEOS and NCAR model simulations we can see that the anomalous easterlies over Amazon are deflected by the Andes. The southern branch produces positive rainfall anomalies downstream south of 20°S, but the strength of the anomalous flow is too weak and the position of the rainfall anomaly too far from the observed.

As discussed in LZ, the SASM has two types of rainfall anomaly in response to El Niño. One is directly related to the Walker cell shift, caused by the SST warming in the central-eastern Pacific. The rainfall anomalies over the Ecuador coast and the north-northeast Brazil are mainly in response to this type of anomaly. Another type of the impact is made indirectly via regional feedback processes and interactions with topography and the SASM system, *e.g.* the LLJ east of the Andes, as well as with mid-latitude systems. The above model simulation results suggest that the direct response may be more deterministic and predictable; while the indirect response,

which involves internal dynamics, may be more chaotic and unpredictable. To investigate this issue, Fig. 16 shows the frequency distribution of DJF monthly rainfall simulation over the rainfall anomaly center areas. These areas are: northern Brazil and the western north equatorial Atlantic (Region I; 60°-35°W, 0°-8°N), Ecuador coast and its nearby ocean (Region II; 95°-80°W, 8°S-4°N) and Uruguay-Northeastern Argentina and Southern Brazil (Region III; 65°-48°W, 34°-26°S). For each area we plot the frequency distribution weighted by the corresponding precipitation amount, using monthly rainfall on every grid of all ten runs with different initial conditions.

As we discussed in the previous section, the Region I and II are mainly under the influence of the Walker cell shift, which is directly induced by the El Niño warming. For 1997/98 all six-model simulations show significant decrease of heavy rainfall frequencies in Region I and increase in Region II. The ensemble means (Fig.16 (a) and (b)) reveal distinct shift of the frequency peeks in both regions. The spread of individual simulations about the ensemble mean, indicated by the shadings and bars of standard deviation for 1996/97 and 1997/98, respectively, are also well separated. This demonstrates the ensemble predictive skill for these two regions is high. For Region III, where the rainfall anomaly involves more internal dynamis, the model precipitation distributions are unchanged during the 1996/97 El Niño (Fig.16 (c)). This characteristic of model dependency suggests the predictive skill over Region III by the models is severely limited. From this study, it is not clear that how much error is due to the chaotic nature of the flow system and how much error remained caused by model inadequate resolution and problems in physical parameterization. The latter could be improved by increasing model resolution and using superensemble technique (Krishnamurti *et al.* 2000).

El Niño, which shows global wave train patterns, is also well captured by the model ensemble simulation. The simulated pattern is smoother and weaker than the observed. The spatial phase of the PSA pattern over South America and the South Atlantic differs substantially from observation, and may have caused problems in the simulation of the South Atlantic high.

A serious problem common to all model simulations is the misrepresentation of the enhancement of the northwesterly LLJ along the eastern foothills of the Andes. In this aspect, model results are highly divergent. Due to lack of moisture transport from the Amazon basin by the anomalous northwesterly LLJ, the positive rainfall anomaly center observed over the Uruguay-Southern Brazil area is largely missing in all six GCM simulations. An assessment of the predictability of regional rainfall anomaly shows promising skill over Ecuador coast and to a lesser degree over northern Brazil. Both are directly under the influence of the Walker cell shift in response to the SST warming in the eastern-central Pacific. The model predictability of rainfall anomalies over the subtropical southeast of South America is very low. This is because the subtropical rainfall anomaly is generated by the El Niño induced regional feedback processes and complex interactions with subcomponents of SASM and mid-latitude systems, which are dependent on the internal dynamics of the SASM.

The above results are preliminary, since the data used in this study is only for a two-year period (from 1 September 1996 to 31 August 1998) and also for a limited number of variables. As abundantly clear in the results, the model resolution used in this study is inadequate for simulation of the regional aspects of the SASM. In addition, two important issues were not addressed from this study. One is the impact of the model systematic errors on predictability. Another issue is the origin of the intra-ensemble spread of the model simulations of the LLJ east of the Andes. It is not clear if it reflects model-formulation differences or the hydrodynamic instabilities existed in the monsoon region. These issues need further investigation.

Acknowledgments. We thank the CLIVAR Asian-Australian Monsoon Atmospheric Model Intercomparison Project for providing us the data used in this study. This research is supported by the NASA Earth Science Enterprise, Global Modeling and Analysis Program.

REFERENCES

Aceituno, P., 1988: On the functioning of the Southern Oscillation in the South American sector. Part I: Surface climate. *Mon. Wea. Rev.*, **116**, 505-524.

Berbery, E.H., and E.A. Collini, 2000: Springtime precipitation and water vapor flux convergence over southeastern South America. *Mon. Wea. Rev.*, **128**, 5, 1328-1346.

Bonan, G.B., 1998: The land surface climatology of the NCAR land surface model (LSM 1.0) coupled to the NCAR Community Climate Model (CCM3). *J. Climate*, **11**, 1307-1326.

Campana, K.A., Y.-T. Hou, K.E. Mitchell, S.-K. Yang, and R. Cullather, 1994: Improved diagnostic cloud parameterization in NMC's global model. Preprints of the 10th Conference on Numerical Weather Prediction, Portland, OR, American Meteorological Society, 324-325.

Chou, M.-D., 1992: A solar-radiation model for use in climate studies. *J. Atmos. Sci.*, **49**, 762-772.

———, and M.J. Suarez, 1994: An efficient thermal infrared radiation parameterization for use in general circulation models. NASA Tech. Memo., No. 104606, Vol. 3, Goddard Space Flight Center, Greenbelt, MD 20771.

Deardorff, J.W., 1978: Efficient prediction of ground surface-temperature and moisture, with inclusion of a layer of vegetation. *J. Geophys. Res.*, **83**, 1889-1903.

Douglas M, Nicolini M, Saulo C. 1999. The low-level jet at Santa Cruz, Bolivia during January-March 1998 pilot balloon observations and model comparisons. In AMS Preprints, 10th Symposium on Global Change Studies, 10-15 January 1999, Dallas, Texas; 223-226.

Fels, S.B., and Schwarzkopf, M.D., 1975: Simplified exchange approximation – New method for radiative-transfer calculations. *J. Atmos. Sci.*, **32**, 1475-1488.

Folland, C.K., and D.E. Parker, 1995: Correction of instrumental biases in historical sea-surface temperature data. *Q. J. Roy. Meteor. Soc.*, **121**, 319-367.

Garreaud, R.D., and J.M. Wallace, 1998: Summertime incursions of midlatitude air into subtropical and tropical South America. *Mon. Wea. Rev.*, 126, 2713-2733.

Gates, W.L., J.S. Boyle, C. Covey, C.G. Dease, C.M. Doutriaux, R.S. Drach, M. Fiorino, P.J. Gleckler, J.J. Hnilo, S.M. Marlais, T.J. Phillips, G.L. Potter, B.D. Santer, K.R. Sperber, K.E. Taylor, and D.N. Williams, 1999: An overview of the results of the atmospheric model intercomparison project (AMIP1). *Bull. Amer. Meteor. Soc.*, **80**, 29-55.

Gordon, C.T., 1992: Comparison of 30 day integrations with and without cloud-radiation interaction. *Mon. Wea. Rev.*, **120**, 1244-1277.

Grimm, A.M., V.R. Barros, and M.E. Doyle, 2000: Climate variability in southern South America associated with El Niño and La Niña events. *J. Cliamte*, **13**, 35-58.

Harshvardhan, R. Davies, D.A. Randall, and T.G. Corsetti, 1987: A fast radiation parameterization for general circulation models. *J. Geophys. Res.*, **92**, 1009-1016.

Hou, Y.-T., 1990: Cloud-radiation-dynamics interaction. Ph.D. Dissertation, University of Maryland at College Park, 209 pp.

Kalnay, E., and Co-authors 1996: The NCEP/NCAR 40-year reanalysis project. *Bull. Amer. Meteor. Soc.*, **77**, 437-471.

Kang, I.-S., K. Jin, K.-M. Lau, J. Shukla, V. Krishnamurthy, S.D. Schubert, D.E. Wailser, W.F. Stern, V. Satyan, A. Kitoh, G.A. Meehl, M. Kanamitsu, V.Ya. Galin, J.-K. Kim, Akimasa Sumi, G. Wu, and Y. Liu, 2002: Intercomparison of GCM simulation anomalies associated with the 1997-98 El Niño. *Bull. Amer. Meteor. Soc.*, submitted

Kiehl, J.T., 1994: On the observed near cancellation between longwave and shortwave cloud forcing in tropical regions. *J. Climate*, **7**, 559-565.

———, J.J. Hack, G. Bonan, B. Boville, D. Williamson, and P. Rasch, 1998: The national center for atmospheric research community climate model (CCM3). *J. Climate*, **11**, 1131-1149.

Kousky, V.E., M.T. Kagano and I.F.A. Cavalcanti, 1984: A review of the Southern Oscillation: oceanic-atmospheric circulation changes and related rainfall anomalies. *Tellus*, **36A**, 490-504.

Krishnamurti, T.N., C.M. Kishtawal, D.W. Shin, and C.E. Williford, 2000: Improving tropical Prediction forecasts from a multianalysis superensemble. *J. Climate*, **13**, 4217-4227.

Lau, K.-M., and J. Zhou, 2002: Responses of the South American Summer Monsoon climate system to ENSO during 1997-99. Submitted to *Int. J. of Climatol.*

Lacis, A.A., and J.E. Hansen, 1974: A parameterization for the absorption of solar radiation in the earth's atmosphere. *J. Atmos. Sci.*, **31**, 118-133.

Liebmann, B., G.N. Kiladis, J.A. Marengo, T. Ambrizzi, and J.D. Glick, 1999: Submonthly convective variability over South America and the South Atlantic convergence zone, *J. Climate*, **12**, 1877-1891.

Mo, K.C., and J. Nogués-Paegle, 2001: The Pacific-South American modes and their downstream impacts. *Int. J. of Climatol.*, **21**, 1211-1229.

Moorthi, S., and M.J. Suarez, 1992: Relaxed Arakawa-Schubert - A parameterization of moist convection for general-circulation models. *Mon. Wea. Rev.*, **120**, 978-1002.

Nobre, P., A.D. Moura and L. Sun, 2001: Dynamical downscaling of seasonal climate prediction over Nordeste Brazil with ECHAM3 and NCEP's regional spectral models at IRI. *Bull. Amer. Meteor. Soc.*, **82**, 2787-2796.

Nogués-Paegle, J., R. Fu, E. H. Berbery, W. C. Chao, T.-C. Chen, K. Cook, D. Enfield, R. Ferreira, V. Kousky, B. Liebmann, K. Mo, J. D. Neelin, J. Paegle, A. Robertson, A. Seth, J. Zhou, 2002: Progress in Pan American CLIVAR Research: Understanding the South American Monsoon. *Meteorologica*, submitted.

———, L.A. Byerle, and K.C. Mo, 2000: Intraseasonal modulation of South American summer precipitation, *Mon. Wea. Rev.*, **128**, 837-850.

Paegle, J., 1998: A comparative review of South American low-level jets. *Meteorologica*, **23**, 73-81.

Pan, H.-L., and L. Mahrt, 1987: Interaction between soil hydrology and boundary layer developments. *Boundary Layer Meteor.*, **38**, 185-202.

Ropelewski, C.F., and M.S Halpert, 1987: Global and regional scale precipitation patterns associated with the El Niño / Southern Oscillation. *Mon. Wea. Rev.*, **115**, 1606-1626.

Schemm, J.-K., S. Schubert, J. Terry, S. Bloom, and Y. Sud, 1992: Estimates of monthly mean soil moisture for 1979-89, NASA Tech. Memo., No. 104571, Goddard Space Flight Center, Greenbelt, MD 20771.

Schwarzkopf, M.D., and S.B. Fels, 1991: The simplified exchange method revised - An accurate, rapid method for computation of infrared cooling rates and fluxes. *J. Geophys. Res.*, **96**, 9075-9096.

Shukla, J., and M.J. Fennessy, 1994: Simulation and predictability of monsoons. Proceedings of the International Conference on Monsoon Variability and Prediction. Tech. Rep. WCRP-84, 567-575.

Slingo, J.M., and B. Ritter, 1985: Cloud prediction in the ECMWF model. ECMWF Tech. Report., No. 46, European Center for Medium-Range Weather Forecasts, Reading, England, 48pp.

———, J.M., 1987: The development and verification of a cloud prediction model for the ECMWF model. *Quart. J. Roy. Meteor. Soc.*, **13**, 899-927.

Sud, Y.C., and G.K. Walker, 1992: A review of recent research on improvement of physical parameterizations in the GLA GCM. In *Physical Processes in Atmospheric Models*, D.R. Sikka and S.S. Singh (eds.), Wiley Eastern Ltd., New Delhi, 422-479.

Uvo, C.B., C.A. Repelli, S.E. Zebiak, and Y. Kushnir, 1998: The relationship between tropical Pacific and Atlantic SST and Northeast Brazil monthly precipitation. *J. Climate*, **11**, 551-562.

Virji, H., 1981: A preliminary study of summertime tropospheric circulation patterns over South America estimated from cloud winds. *Mon. Wea. Rev.*, **109**, 167-178.

Wallace, J.M., and D.S. Gutzler, 1981: Teleconnections in the geopotential height field during the Northern Hemisphere winter. *Mon. Wea. Rev.*, 109, 784-812.

Xie, P., and P.A. Arkin, 1997: Global Precipitation: A 17-year monthly analysis based on gauge observations, satellite estimates, and numerical model outputs, *Bull. Am. Meteorol. Soc.*, **78**, 2539-2558.

Xue, Y.-K., P.J. Sellers, J.L. Kinter II, and J. Shukla, 1991: A simplified biosphere model for global climate studies. *J. Climate*, **4**, 345-364.

Zhang, G.J., and N.A. McFarlane, 1995: Sensitivity of climate simulations to the parameterization of cumulus convection in the Canadian Climate Centre general circulation model. *Atmos.-Ocean*, **33**, 407-446.

Zhou, J., and W.K.-M. Lau, 1999: Summertime Intraseasonal Variability over South America, *Proceedings of the 24th Annual Climate Diagnostics and Prediction Workshop*, 5-9 November 1999, Tucson, Arizona, 299-302.

———, and W.K.-M. Lau, 2001: Principal modes of interannual and decadal variability of summer rainfall over South America. *Int. J. of Climatol.*, **21**, 1623-1644.

TABLE AND FIGURE CAPTIONS

Table 1 Description of the models used in this study (From Kang *et al.* 2002).

Figure 1 Climatology of 850-hPa wind (m/s) and SLP (hPa), showing the annual mean and DJF departure from the annual mean from top to bottom panel and NCEP reanalysis and the difference between the ensemble simulation and NCEP reanalysis from left to right panel.

Figure 2 Hovmoller diagram, showing annual cycle of 850-hPa meridional wind (m/s) along 15°S. (a) NCEP reanalysis and (b) model ensemble simulation. The shading indicates the standard deviation among model climatologies.

Figure 3 Hovmoller diagram, showing annual cycle of meridional wind at 15°S, 42.5°W (left) and at 15°S, 62.5°W (right) for NCEP reanalysis (top) and the model ensemble simulation (bottom).

Figure 4 Seasonal rainfall climatology (cm) of CMAP rainfall analysis (top) and the ensemble simulation error (bottom) for SON (left), DJF (middle) and MAM (right).

Figure 5 Individual model simulation error (cm) of DJF rainfall.

Figure 6 Climatology of the allocation of seasonal rainfall (percentage of the annual sum) for SON (left), DJF (middle) and MAM (right). From top to bottom are CMAP rainfall analysis and GCM ensemble simulation.

Figure 7 Seasonal rainfall advancement (upper) and withdrawal (lower) described by 6 mm/day contour. From left to right are CMAP rainfall analysis and the ensemble simulation.

Figure 8 Vertical-zonal cross-section of 1997/98 DJF temperature anomaly (°K) along 15°S. From top to bottom are NCEP reanalysis and the ensemble model simulation. The shading indicates the standard deviation among model simulations.

Figure 9 Same as Fig. 8 except for individual model simulations.

Figure 10 1997/98 DJF 200-hPa geopotential height anomaly (gpm). From top to bottom are NCEP reanalysis and the difference of the ensemble simulation minus NCEP reanalysis, respectively. The shading indicates the standard deviation among model simulations.

Figure 11 1997/98 DJF wind (m/s) and streamline anomalies at 200-Pa (top) and 850-Pa (bottom). From left to right are NCEP reanalysis and the model ensemble simulation, respectively.

Figure 12 Vertical-meridional cross-section of 1997/98 DJF zonal wind anomaly zonally averaged between 80°-50°W (m/s). From left to right are NCEP reanalysis and the model ensemble simulation respectively. The shading indicates the standard deviation among model simulations.

Figure 13 Same as Fig. 12, except for the vertical-zonal cross-section of 1997/98 DJF meridional wing anomaly along 15°S.

Figure 14 1997/98 DJF CMAP rainfall (mm/day) and NCEP reanalysis 850-Pa wind (m/s) anomalies (left) and the corresponding model ensemble simulations (right). The wind vectors are bolded, when the speed exceeds 2 m/s.

Figure 15 Same as Fig. 14 except for the simulations by individual model.

Figure 16 The DJF monthly rainfall frequency distributions, weighted by the rainfall rate, over (a) Region I (65°-47.5°W, 34°-26°S), (b) Region II (95°-80°W, 8°S-4°N), and (c) Region III (65°-47.5°W, 34°-26°S). The dash and solid lines are indications of 1996/97 and 1997/98, respectively. The shadings and bars are standard deviations among model simulations for 1996/97 and 1997/98, respectively.

Group	Model	Institution	Resolution	Radiation	Convection	Land Surface Process	Cloud Formulation
COLA	COLA 1.11	Center for Ocean-Land-Atmosphere Studies	R40 L18 (128x102)	Lacis and Hansen (74) Harshvardhan *et al.* (87)	Relaxed Arakawa-Schubert	SSiB model Xue *et al.* (91)	Hou (90) based on Slingo (87)
GEOS	GEOS-2	NASA/Goddard Space Flight Center	2.5°x2° L43 (144x91)	Chou and Suarez (94)	RAS (Moorthi and Suarez 92)	Schemm *et al.* (92)	Slingo and Ritter (85)
GFDL	DERF GFDLSM V197	Geophysical Fluid Dynamics Laboratory	T42 L18 (128x64)	Lacis and Hansen (74) Schwarzkopf and Fels (91)	RAS (Moorthi and Suarez 92)	Deardorff (78)	Slingo (87) Gordon (92)
NCAR	CCM3	National Center for Atmospheric Research	T42 L18 (128x64)	Kiehl *et al.* (98)	Mass flux scheme (Zhang and McFarlane 95)	Land surface model (Bonan 98)	Slingo (87) Kiehl (94)
NCEP	Seasonal MRF vsn0	National Center for Environmental Prediction	T42 L28 (128x64)	Chou (92) Fels and Schwarzkopf (75)	RAS (Moorthi and Suarez 92)	Pan and Mahrt (87)	Slingo (87) Campana *et al.* (94)
SUNY/GLA	GLA GCM – 01.0	State University of New York	5°x4° L17 (72x46)	Harshvardhan *et al.* (87)	Modified Arakawa-Schubert	Deardorff (78)	Sud and Walker (92)

Table 1

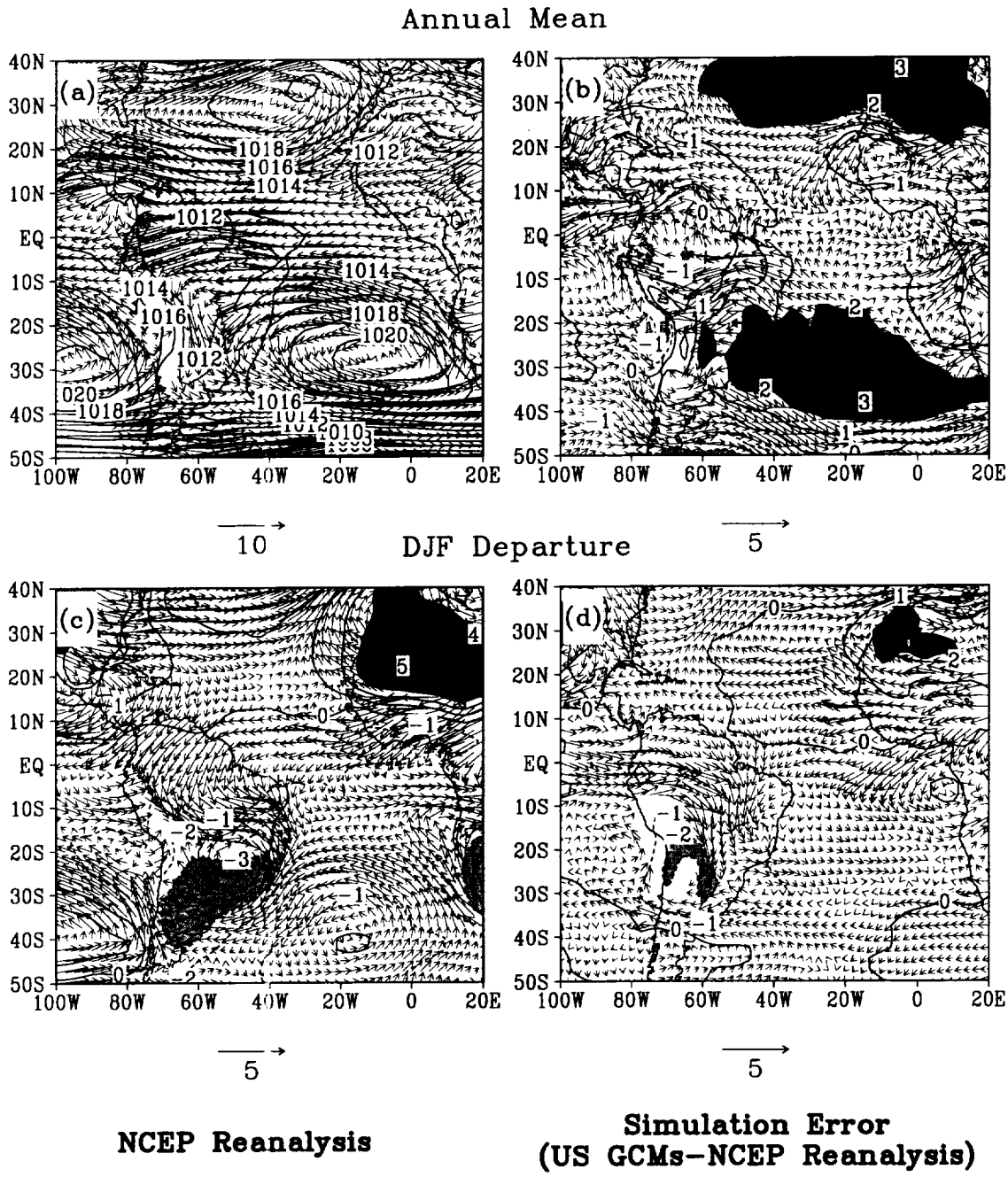
Annual Mean
(a)
(b)
DJF Departure
(c)
(d)
40N
30N
20N
10N
EQ
10S
20S
30S
40S
50S
100W
80W
60W
40W
20W
0
20E
10
5
5
5
NCEP Reanalysis
Simulation Error
(US GCMs–NCEP Reanalysis)

Fig. 1

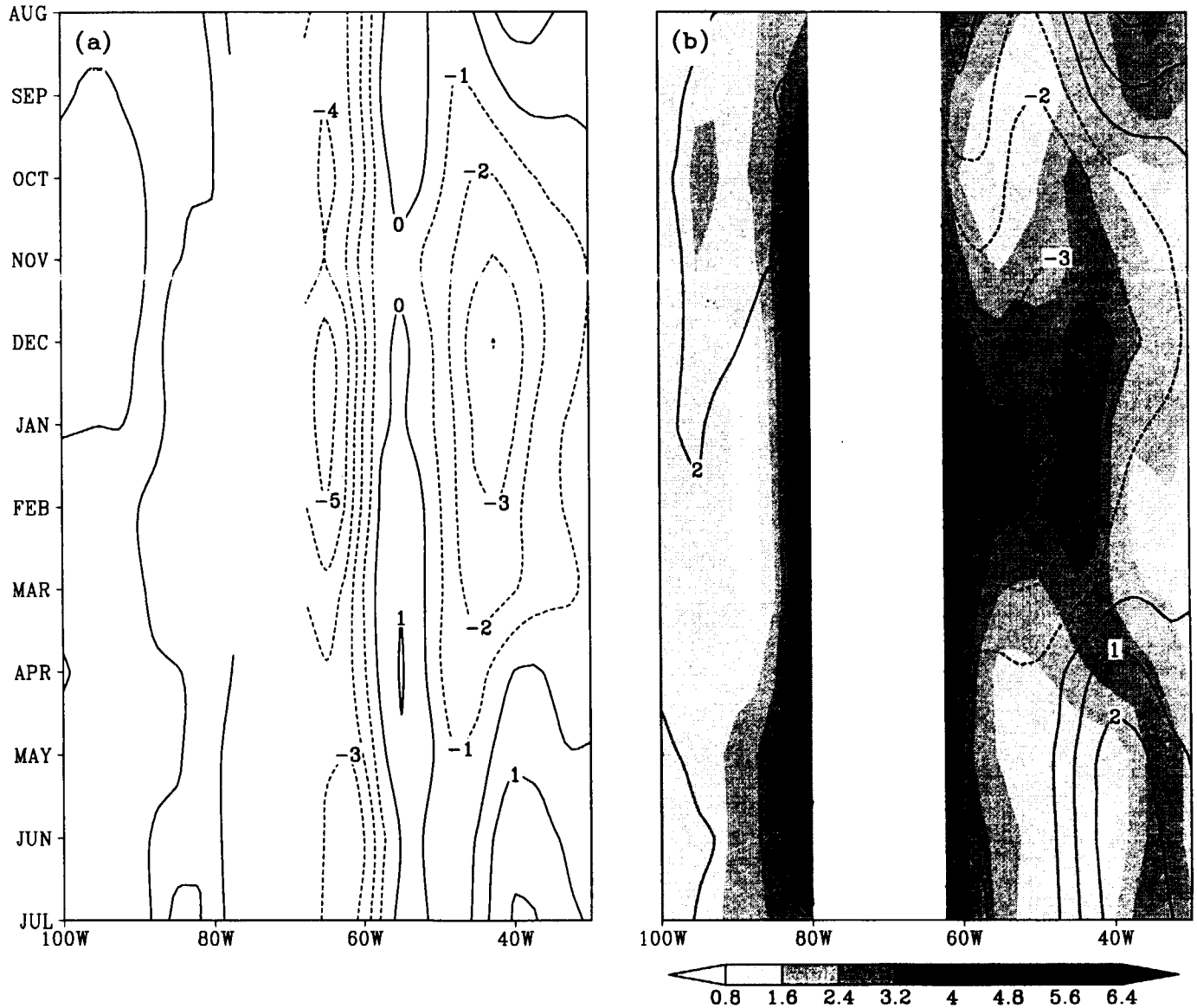
(a)
AUG
SEP
OCT
NOV
DEC
JAN
FEB
MAR
APR
MAY
JUN
JUL
100W
80W
60W
40W
-4
-1
-2
0
0
-5
-3
1
-2
-1
-3
1
(b)
-2
-3
2
1
2
100W
80W
60W
40W
0.8
1.6
2.4
3.2
4
4.8
5.6
6.4

Fig. 2

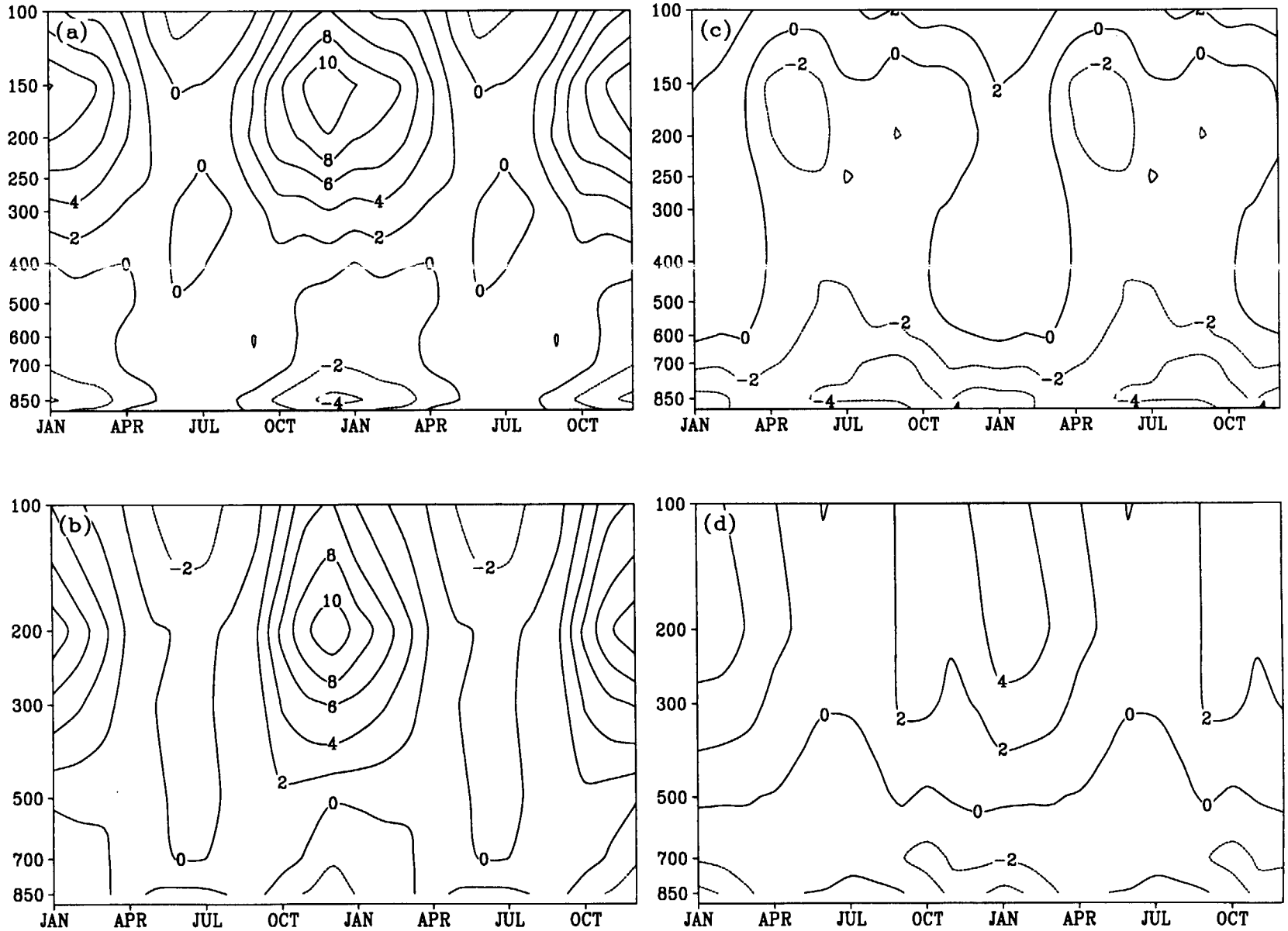

Fig. 3

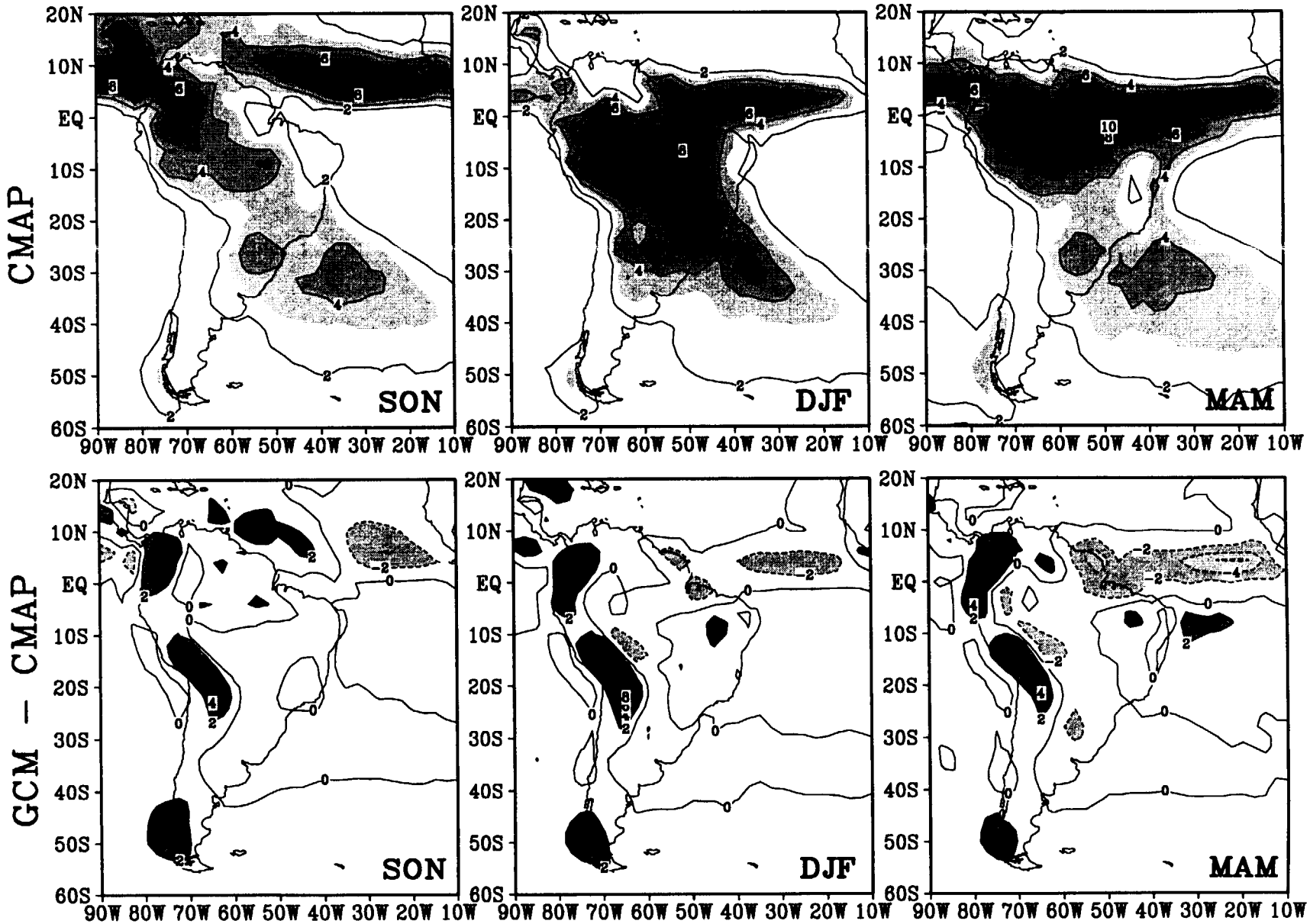
CMAP
GCM − CMAP
SON
DJF
MAM
20N
10N
EQ
10S
20S
30S
40S
50S
60S
90W 80W 70W 60W 50W 40W 30W 20W 10W

Fig. 4

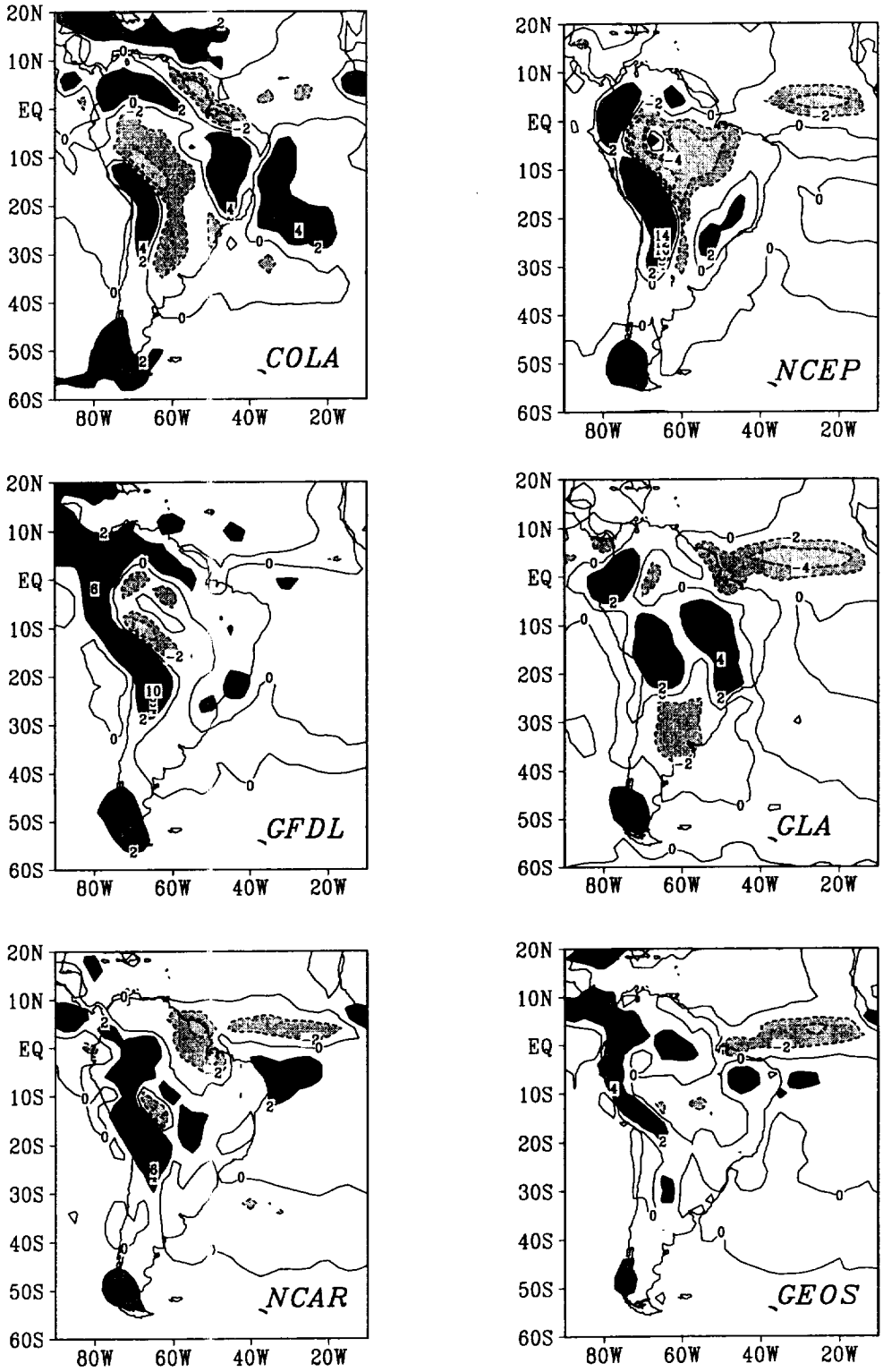
COLA
NCEP
GFDL
GLA
NCAR
GEOS
20N
10N
EQ
10S
20S
30S
40S
50S
60S
80W
60W
40W
20W

Fig. 5

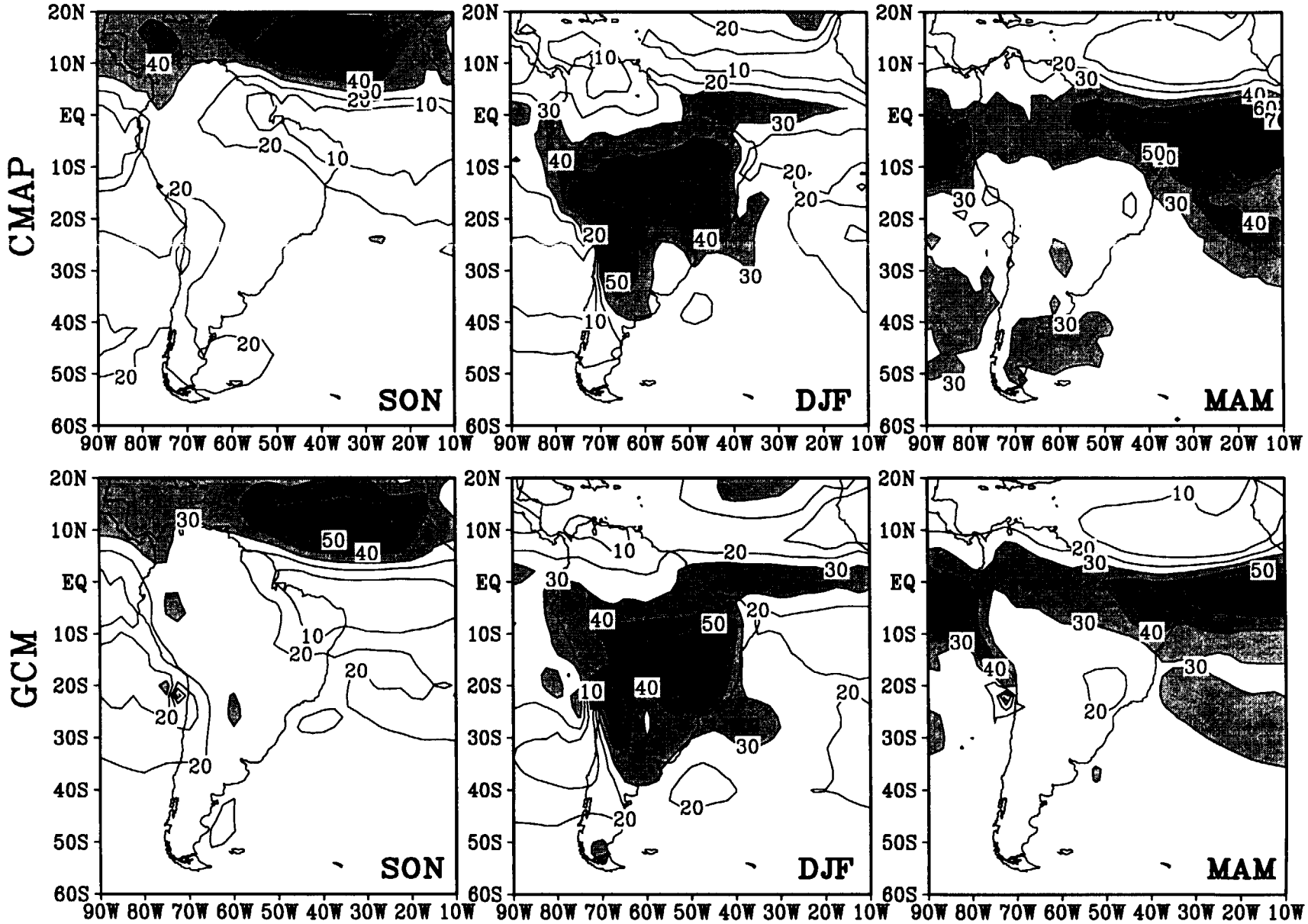
CMAP
GCM
SON
DJF
MAM
20N
10N
EQ
10S
20S
30S
40S
50S
60S
90W 80W 70W 60W 50W 40W 30W 20W 10W

Fig. 6

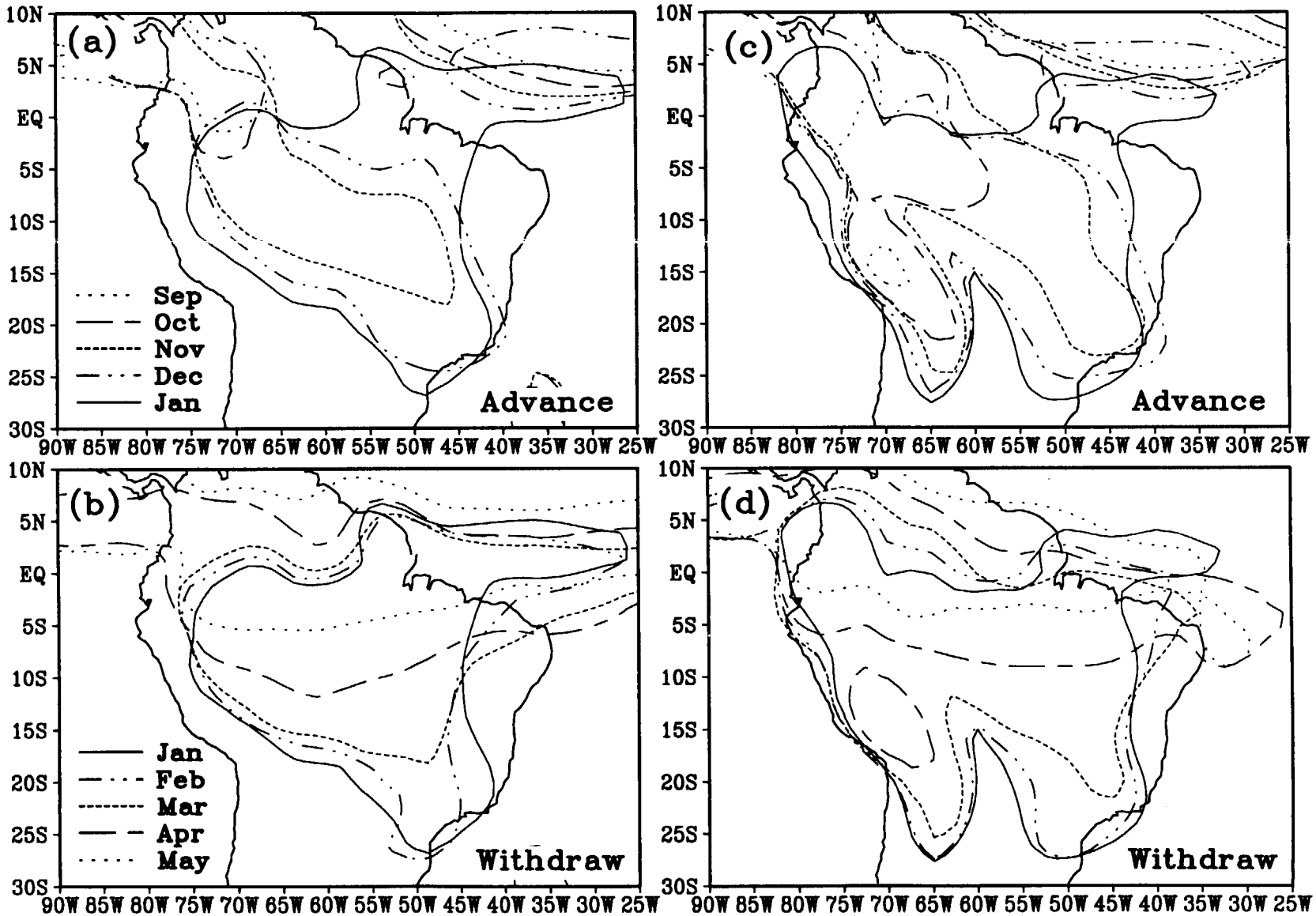
(a)
(b)
(c)
(d)
Sep
Oct
Nov
Dec
Jan
Feb
Mar
Apr
May
Advance
Withdraw
10N
5N
EQ
5S
10S
15S
20S
25S
30S
90W 85W 80W 75W 70W 65W 60W 55W 50W 45W 40W 35W 30W 25W
CMAP
GCM

Fig. 7

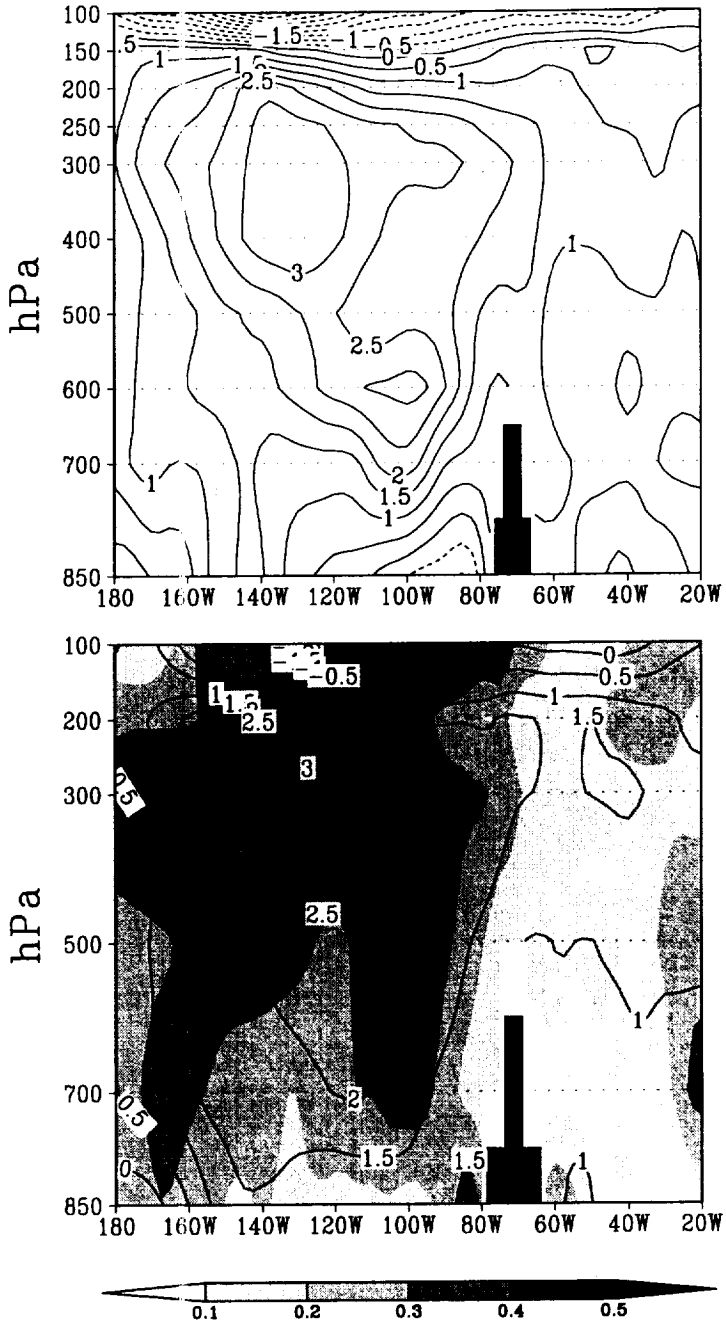
hPa
100
150
200
250
300
400
500
600
700
850
180
160W
140W
120W
100W
80W
60W
40W
20W
0.1
0.2
0.3
0.4
0.5

Fig. 8

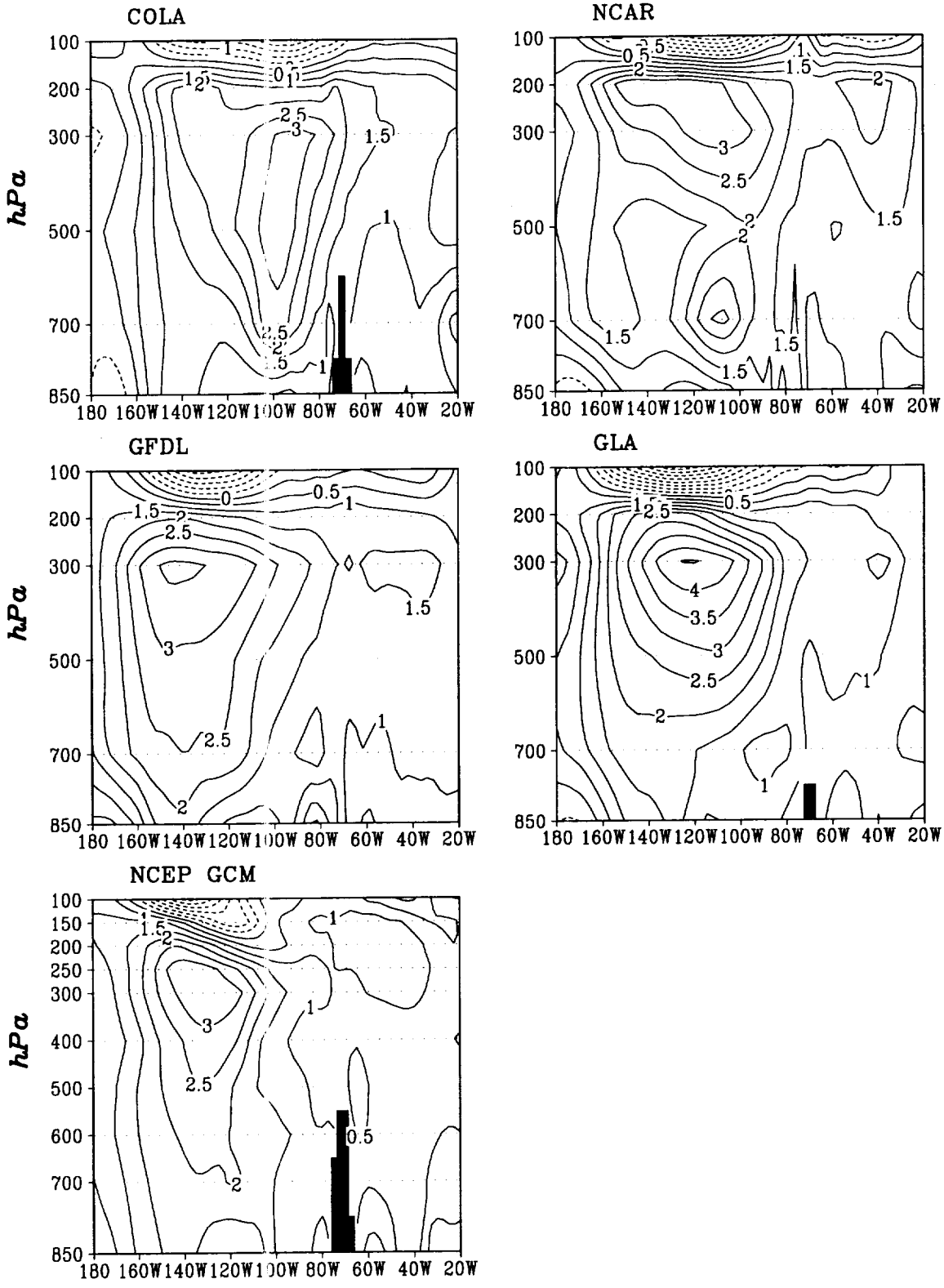
COLA
NCAR
GFDL
GLA
NCEP GCM
hPa
100
200
300
500
700
850
150
250
400
600
180 160W 140W 120W 100W 80W 60W 40W 20W

Fig. 9

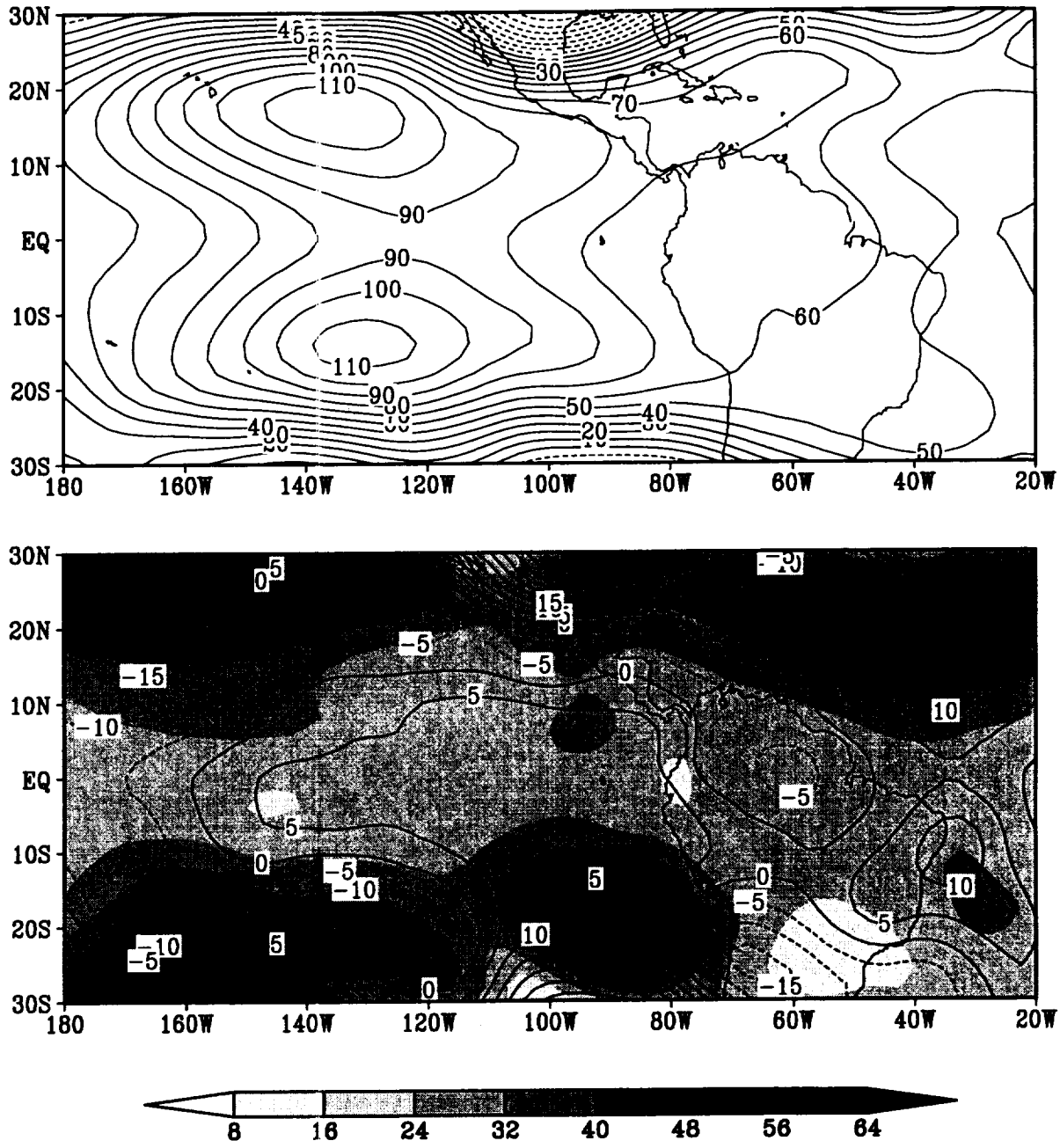
30N
20N
10N
EQ
10S
20S
30S
180
160W
140W
120W
100W
80W
60W
40W
20W
8
16
24
32
40
48
56
64

Fig. 10

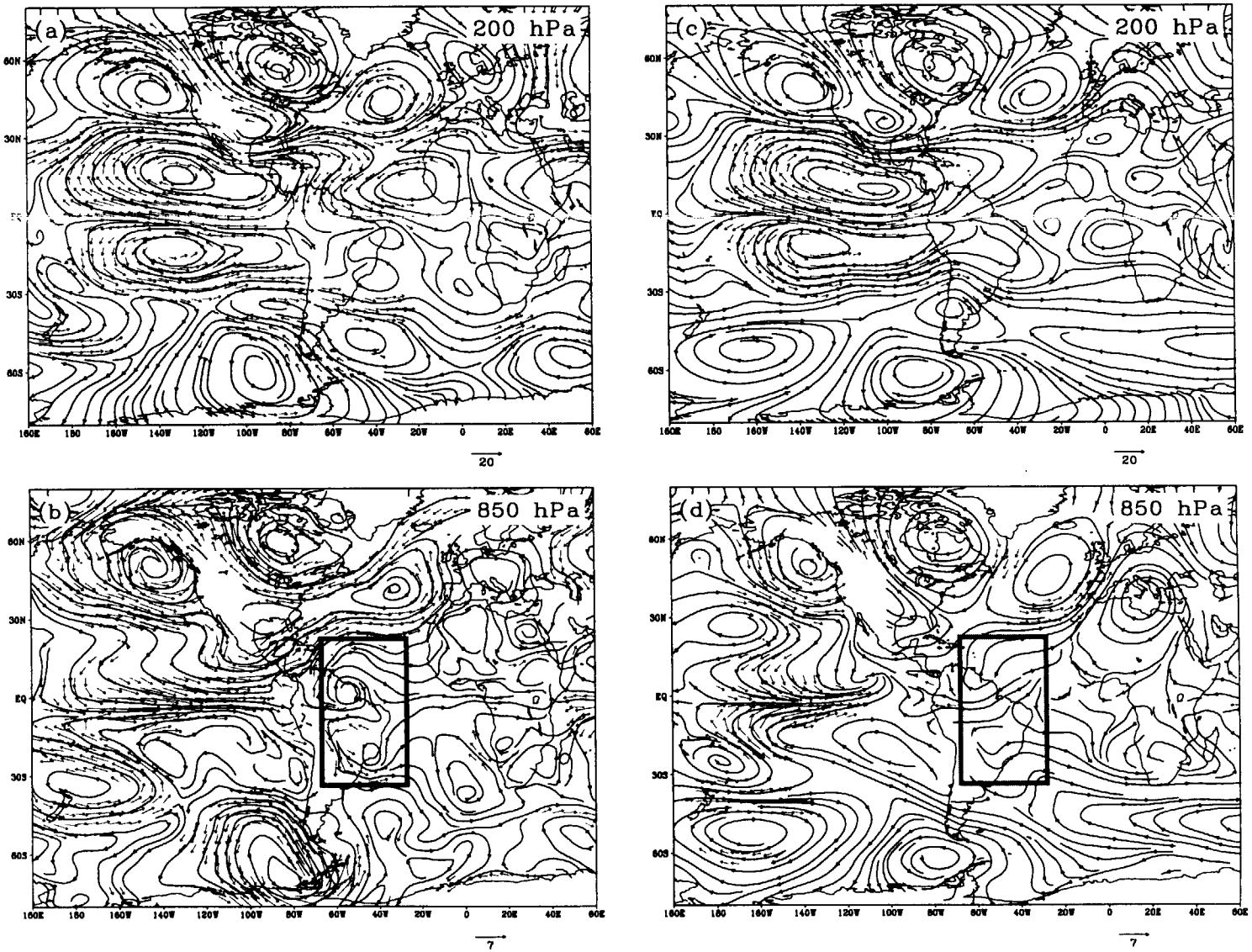
(a)
200 hPa
(c)
200 hPa
(b)
850 hPa
(d)
850 hPa
60N
30N
EQ
30S
60S
160E 180 160W 140W 120W 100W 80W 60W 40W 20W 0 20E 40E 60E
20
7

Fig. 11

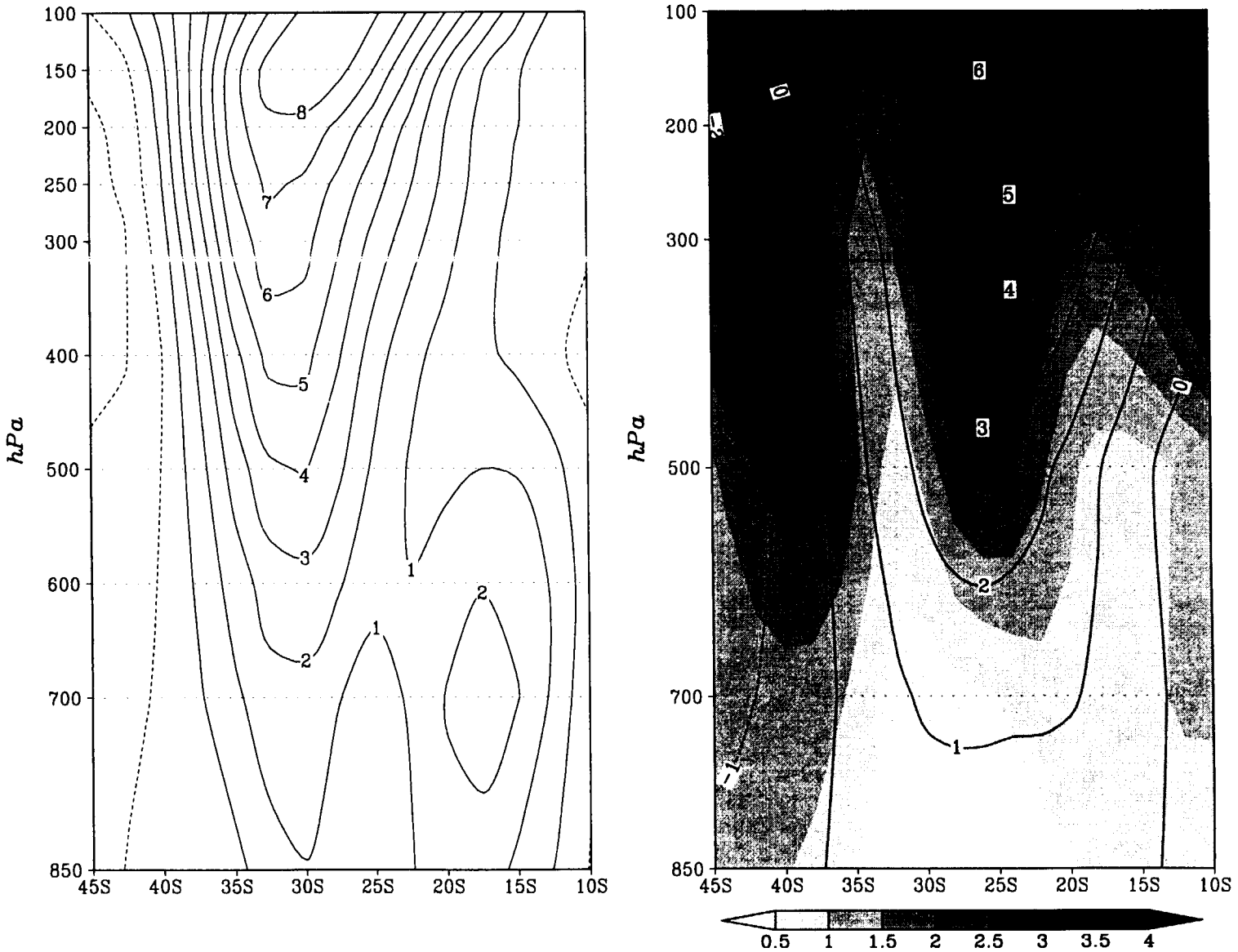
hPa
100
150
200
250
300
400
500
600
700
850
45S
40S
35S
30S
25S
20S
15S
10S
8
7
6
5
4
3
2
1
0
-1
0.5
1
1.5
2
2.5
3
3.5
4

Fig. 12

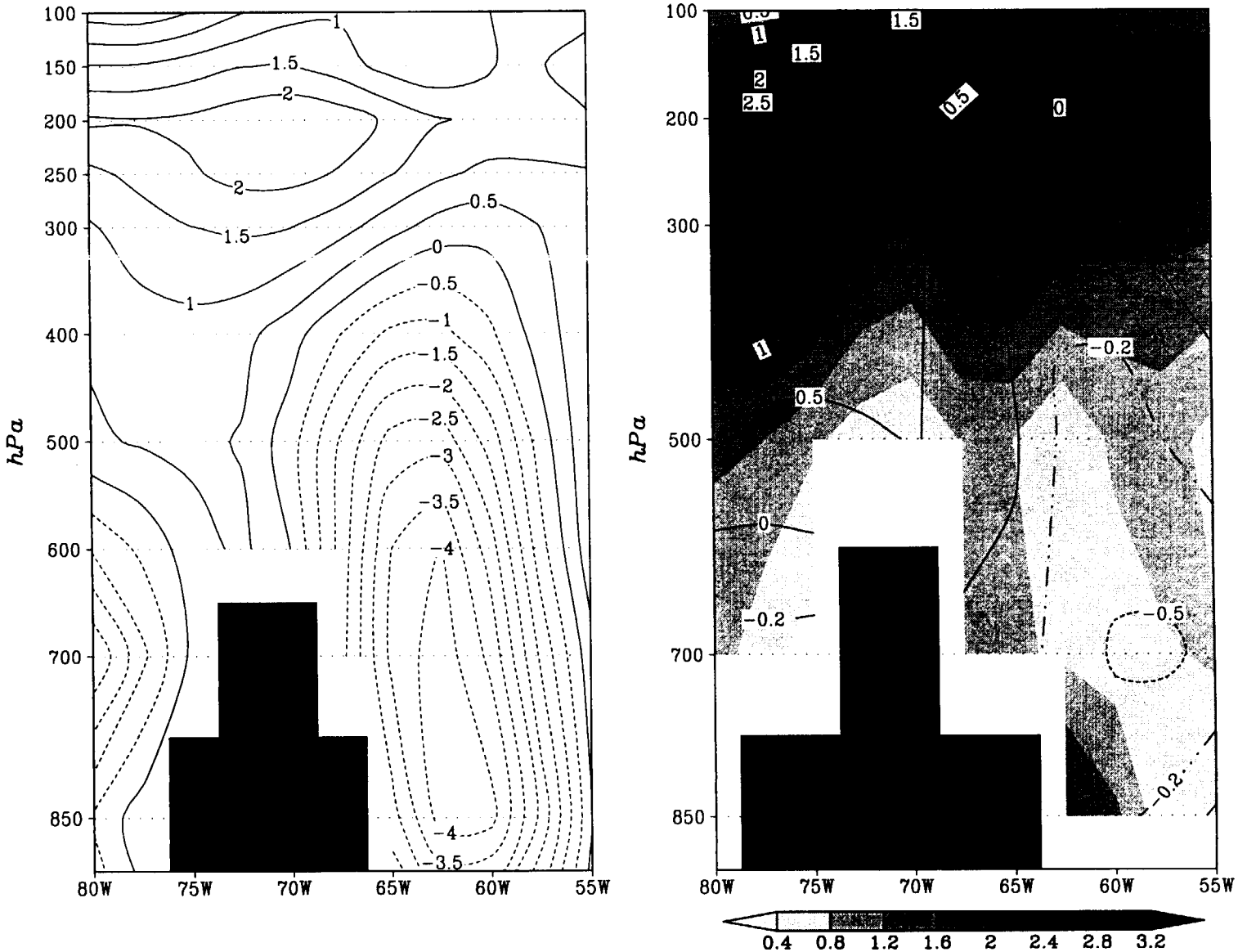
hPa
100
150
200
250
300
400
500
600
700
850
80W
75W
70W
65W
60W
55W
1
1.5
2
2
1.5
0.5
0
-0.5
-1
-1.5
-2
-2.5
-3
-3.5
-4
-4
-3.5
hPa
100
200
300
500
700
850
80W
75W
70W
65W
60W
55W
1.5
1
1.5
2
2.5
0.5
0
1
-0.2
0.5
0
-0.2
-0.5
-0.2
0.4
0.8
1.2
1.6
2
2.4
2.8
3.2

Fig. 13

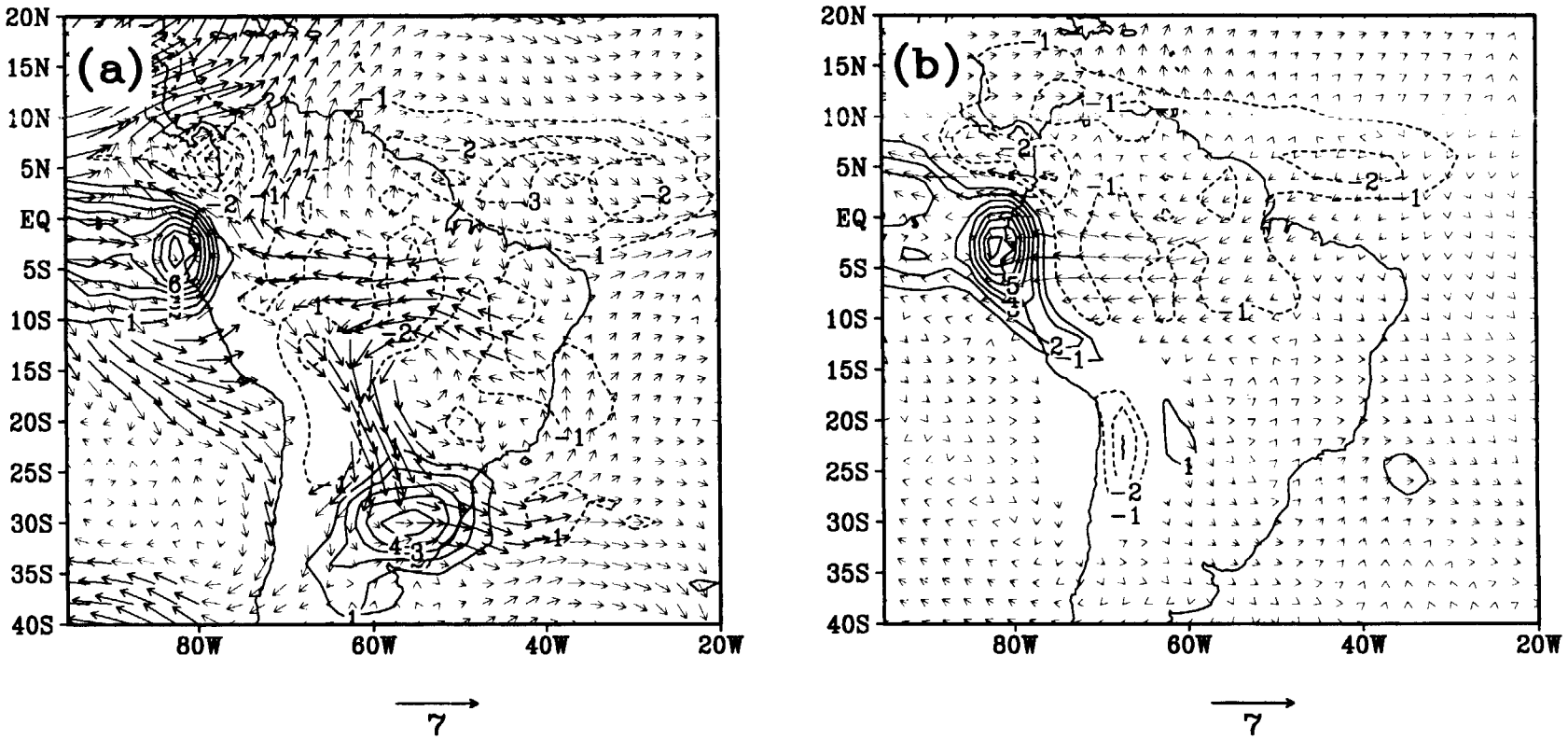
(a)
(b)
20N
15N
10N
5N
EQ
5S
10S
15S
20S
25S
30S
35S
40S
80W
60W
40W
20W
7
7

Fig. 14

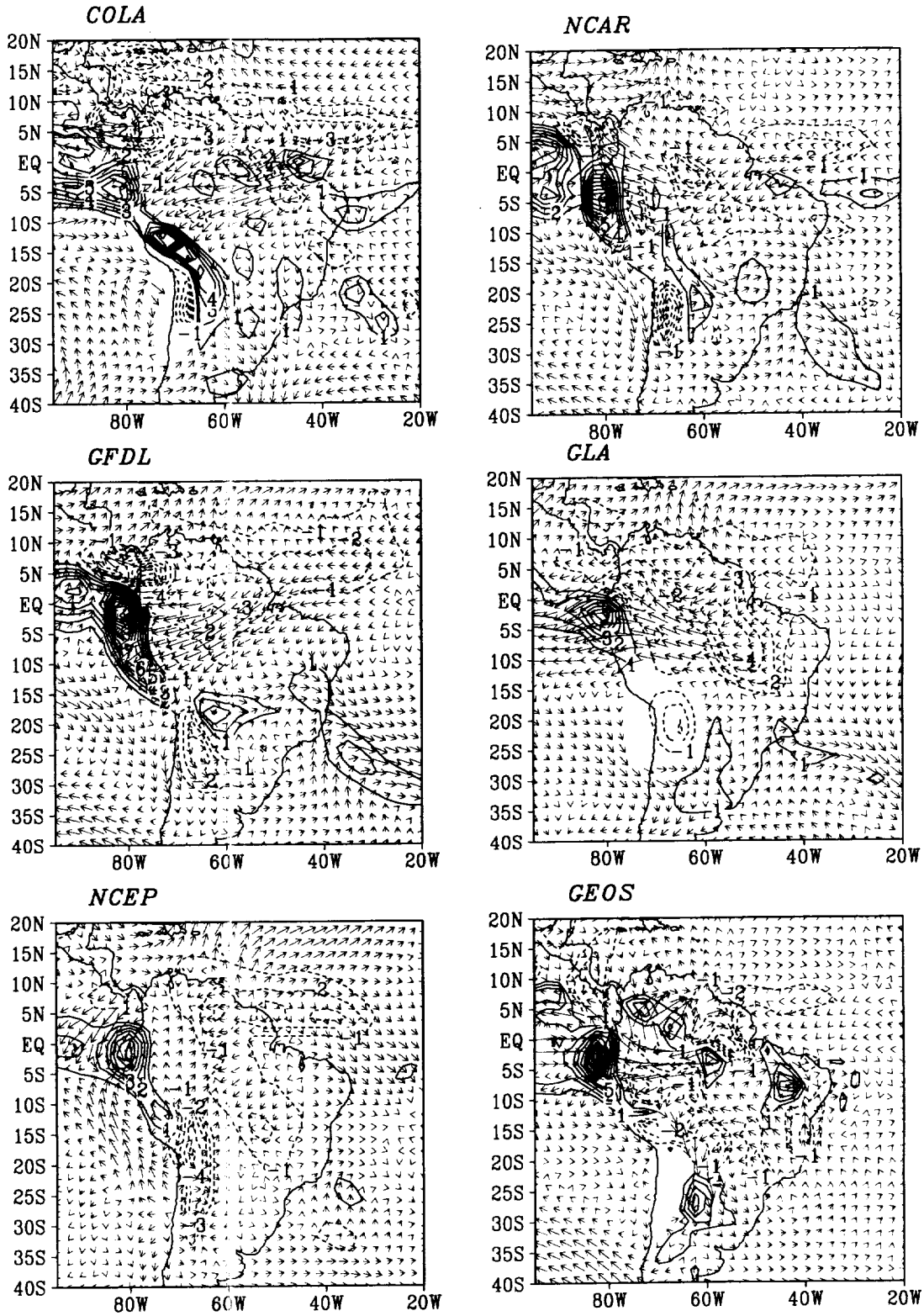
COLA
NCAR
GFDL
GLA
NCEP
GEOS
20N
15N
10N
5N
EQ
5S
10S
15S
20S
25S
30S
35S
40S
80W
60W
40W
20W

Fig. 15

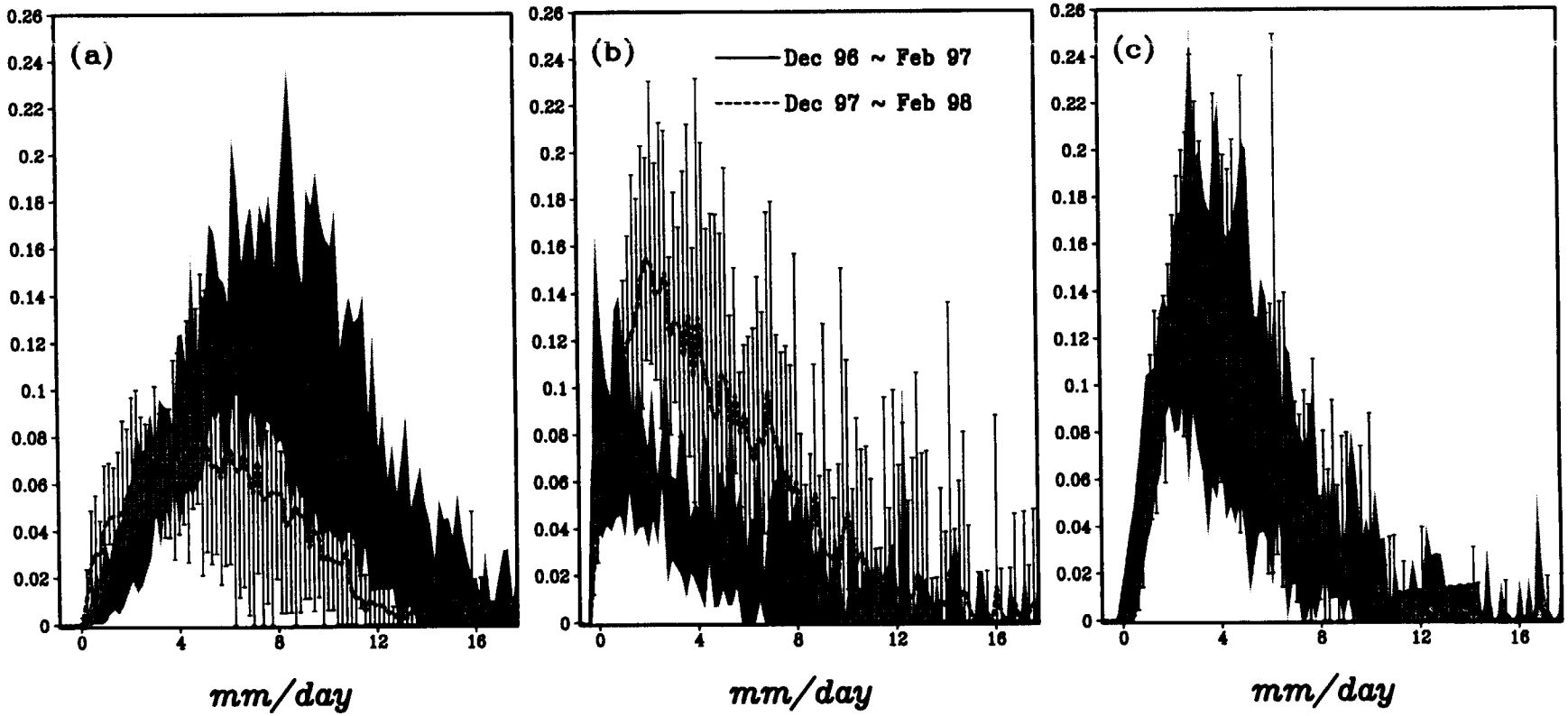
(a)
(b)
(c)
Dec 96 ~ Feb 97
Dec 97 ~ Feb 98
0.26
0.24
0.22
0.2
0.18
0.16
0.14
0.12
0.1
0.08
0.06
0.04
0.02
0
0
4
8
12
16
mm/day

Fig. 16